PCCP

Accepted Manuscript

ROYAL SOCIETY OF CHEMISTRY

www.rsc.org/pccp

Journal Name

RSCPublishing

ARTICLE

Enhancement of near-infrared luminescence of ytterbium in triple-stranded binuclear helicates

Cite this: DOI: 10.1039/x0xx00000x

Bing Li, Hongfeng Li,* Peng Chen, Wenbin Sun, Cheng Wang, Ting Gao and Pengfei Yan*

Received 00th January 2012,
Accepted 00th January 2012

DOI: 10.1039/x0xx00000x

www.rsc.org/

A bis-β-diketone, bis(4,4,4-trifluoro-1,3-dioxobutyl)(2,2'-bithienyl) (BTT), which can be looked upon as coupling of two mono-β-diketone (2-thenoyltrifluoroacetone, TTA) at the 5,5'-position of thiophene ring, has been designed for exploring the advantages of binuclear helical structure on sensitizing the lanthanide NIR luminescence. The Yb(III) ion was selected as luminescence center, and its corresponding mono-β-diketone complex $Yb(TTA)_3(DMSO)$ (**1**) and bis-β-diketone complex $Yb_2(BTT)_3(DMSO)_4$ (**2**) were synthesized and isolated. X-ray crystallographical analysis reveals that bis-β-diketone complex $Yb_2(BTT)_3(DMSO)_4$ adopts a triple-stranded dinuclear structure, in which the two Yb(III) ions are helically wrapped by three ligands, and each Yb(III) ion is eight-coordinated by six oxygen atoms from three ligands and two oxygen atoms from the coordinated DMSO molecules. Whereas, the mono-β-diketone complex $Yb(TTA)_3(DMSO)$ is a mononuclear structure, the central Yb(III) ion is coordinated by seven oxygen atoms from three ligands and a DMSO. The photophysical properties related to the electronic transition are characterized by the absorbance spectra, the emission spectra, the emission quantum yields, the emission lifetimes, and the radiative (k_r) and nonradiative rate constants (k_{nr}). The luminescence quantum yields experiment reveals that the dinuclear complex has about 10 times luminescent enhancement compared with the mononuclear complex. This enhancement mainly benefits from its helical structure, which effectively depresses the nonradiative transition caused by high-energy oscillators in ligands, and the part-encapsulated structure decreases the probability of solvents closing to the metal centers.

Introduction

Near-infrared-luminescent lanthanide ions such as Nd(III), Er(III) and Yb(III) have attracted much interest because of their significant application in optical communication,[1] biomedical analysis,[2] medical imaging and therapy.[3] The forbidden nature of the f–f transition in trivalent lanthanide ions results in a low absorbance coefficients, while inorganic or organic antenna ligands are commonly used to absorb excitation light and transfer energy to the lanthanide in order to achieve bright emission.[4] Compared with the efficient NIR emission of lanthanide ions in inorganic systems, low luminescence quantum yields are commonly observed in the organic lanthanide complexes. This is due to the low-energy excited states of the NIR luminescent lanthanide ions, which is prone to be quenched through multiphonon de-excitation caused by the coupling of high energy oscillators like O–H, N–H and C–H, present in the organic ligands or solvents.[5] Strategies to overcome this problem include: i) Exploit the sterically demanding and/or multidentate ligands that can encapsulate the ion forming the hydrophobic shell around the metal ion,[6] and ii) Replace the ubiquitous C–H bonds with C–D bonds or C–F bonds.[7]

Among the NIR emitters, the Yb(III) undoubtedly is one of the most efficient lanthanide ions, a result of the "clear" excited and ground state levels, and the relatively larger energy gap between them (10 250 cm^{-1}).[8] According to rationally optimize the ligands, the Yb(III) ion will show the highest NIR luminescence quantum yields in lanthanide complexes. Previously, various ligands have been designed for sensitizing the Yb(III) ion NIR luminescence, including macrocyclic porphyrins,[9] coronands,[10] cryptands,[11] cyclens,[12] calixarenes and resorcinarenes;[13] acyclic beta-diketones,[14] quinolinates,[15] terphenyl,[16] polyaminocarboxylates;[17] as well as other chelating agents such as some dyes derivatives,[18] tropolonates,[19] imidophosphinates[20] and boron dipyrromethene (BODIPY).[21] Nevertheless, the luminescence quantum yields observed remain modest, typically in the range of 10^{-3}–10^{-2}, due to the easy quenching by the high energy oscillators present in ligands and solvents. Therefore, clever design of the ligands that can

efficiently depress nonradiative transition is critical for synthesizing high efficient organic lanthanide emitters.

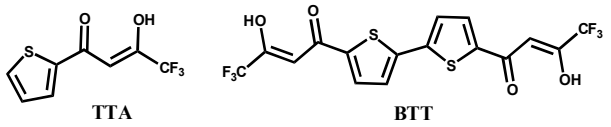

Chart 1 Structures of the ligands TTA and BTT.

Among organic ligands, β-diketones are considered to be better candidate for sensitizing lanthanide ions luminescence, especially for visible light emitting Eu(III) and Tb(III) ions.[22] However, their ability with respect to populating lanthanide ions NIR luminescence seems not to be limited,[23] which is mainly due to the presence of solvents in the coordination sphere of lanthanide ions in the β-diketone complexes. To overcome this, the auxiliary ligands are often employed to replace the solvents.[24] But, it is noted that the ternary complexes often have poor solubility and stability in the solution, which restrict their applications in device processing or bioanalysis area. Therefore, the combination of the efficient sensitization of the beta-diketone to lanthanide ions and the depression of the nonradiative deactivation would be the key for their construction of NIR-emitting organic lanthanide emitter.

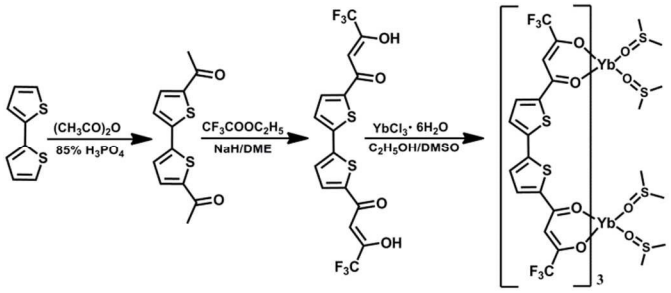

Scheme 1 Synthetic routes of BTT and its complexes $Yb_2(BTT)_3(DMSO)_4$.

In recent years, we, and others, developed several bis-β-diketone ligands, which coordinate to lanthanide ions to form triple-stranded helical structure.[25] Research works by Bünzli and Piguet et al. have revealed that triple-stranded lanthanide helicates assembled about benzimidazole derivatives possess satisfied thermodynamic stability in the solution,[26] which highlights the promising future in bioanalyses and bioimaging. In the reported bis-β-diketonate lanthanide complexes, the dinuclear structure often shows the higher luminescent quantum yields compared with the mononuclear analogue. For instance, Pikramenou et al. reported a samarium bis-β-diketone complex which exhibited 11 times more intense luminescence signal than the corresponding mononuclear analogue.[26f] However, it is not always the case. A recent example reported by us gave a contrasting result that the mononuclear complex showed the higher luminescence quantum yields.[26a] Whereas, the advantages of bis-β-diketone on sensitizing the NIR-emitting lanthanide ions have never been investigated and compared with the mono-β-diketone.

In this paper, we design and synthesize a new bis-β-diketone, bis(4,4,4-trifluoro-1,3-dioxobutyl)(2,2'-bithienyl) (BTT), for the purpose of investigating the advantages of bis-β-diketone as sensitizer for Yb(III) ions NIR luminescence (Scheme 1). The ligand can be looked upon as coupling of two mono-β-diketone (TTA) at the 5,5'-position of thiophene ring (Chart 1). The triple-stranded helical structure of the $Yb_2(BTT)_3(DMSO)_4$ is characterized by single crystal X-ray analysis, and the luminescent properties of the dinuclear complex has been compared with the mononuclear complex $Yb(TTA)_3(DMSO)$. Based on the single crystal structure and the spectral analysis, the factors that enhance emission quantum yields of bis-β-diketonate complex are elucidated in detail.

Results and discussion

Characterization of the ligand and complexes

The synthetic route for ligand BTT and $Yb_2(BTT)_3(DMSO)_4$ are shown in Scheme 1. The ^1H NMR spectrum of BTT obtained at 400 MHz in $CDCl_3$ is shown in Figure S1. The β-diketones generally exhibit keto-enol tautomerism. The amounts of keto- and enol form can be determined by integration of the keto and the enol resonance peaks in the ^1H NMR spectrum. The observed broad single peak at δ 12.09 shows the characteristic H^{enol} protons (Hd), and the singlet at δ 6.99 is assigned to methine H^{keto} protons (Ha). By integrating the areas corresponding to both species, it is found that the ligand exists completely in the enolic form in $CDCl_3$. The observed two double peaks at δ 7.71–7.82 and δ 8.34–8.40 are attributed to the Hc, Hb in thiophene ring, respectively. The double peaks are the results of the spin-spin coupling of the adjacent protons, and being close to the withdrawing carboxyl group make the Hb present at downfield. The FT-IR spectra and microanalysis data demonstrate that the L:Yb mole ratios are 3:1 and 3:2 in **1** and **2**, respectively, and DMSO molecule is present. The carbonyl stretching frequencies of free ligands (TTA, 1612 cm^{-1}; BTT, 1628 cm^{-1}) shift to 1583–15991 cm^{-1} and 1601–1626 cm^{-1}, respectively, thus indicate the coordination of the oxygen atoms to the lanthanide ions. Furthermore, the presence of signals at 1060 $cm^{-1}$and 684–642 cm^{-1} due to the C–S bond confirms the presence of DMSO in two complexes. In addition, the absence of any broad bands around 3500 cm^{-1} in complexes proves that no water molecules are present in the coordination sphere of Yb(III) ions or the crystal lattice. The thermal stability of the complexes was examined by means of thermogravimetric analyses and typical thermograms are depicted in Fig. S2. It is clear from TG curves that **1** firstly undergoes a mass loss of about 8.8% (calcd. 8.5%) between 139 and 187 ºC, corresponding to the loss of one coordinated DMSO. Then, a long plateau is observed until a full decomposition at ca. 280 ºC. In **2**, a mass loss of about 15.6% (calcd 15.7%) corresponding to the loss of four coordinated DMSO is observed in the first step (135−192 ºC). The second step from 280 to 510 ºC corresponds to the thermal

decomposition of the organic ligands, and finally leading to the formation of the stoichiometric amounts of Yb_2O_3.

X-ray crystallographic analysis

In order to obtain accurate structure information, single crystals of **1** and **2** are grown and the molecular structures are determined by single crystal X-ray diffraction (Table S1). The results reveal that **1** and **2** crystallize in the orthogonal space group $P2_12_12_1$ and monoclinic space group $C2/c$, respectively. In the case of **1**, the Yb(III) ion is seven coordinated to one DMSO molecule and three bidentate mono-β-diketonate ligands, as shown in Figure 1(a). The Yb–O distances are in the range of 2.223(9)–2.263(2) Å, while the distance of Yb–O (sulfoxide O atoms) is 2.256 Å.

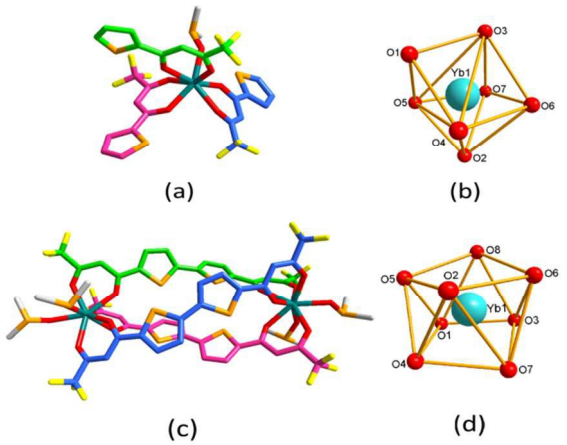

Figure 1 Ball-and-stick representation of the crystal structures of **1** (a), **2** (c) and their coordination polyhedra (b), (d). Ytterbium atoms are shown as cyan spheres, and C atoms in each ligand is represented in different colors.

Complex **2** is a triple-stranded dinuclear helicate featured by the coordination of three bis-β-diketonate ligands to two crystallographically equivalent Yb(III) ions, as shown in Figure 1(c). There are four $Yb_2(BTT)_3(DMSO)_4$ units in the unit cell that each helicate has homochiral Yb(III) centers in either a left-handed Λ–Λ or right-handed Δ–Δ helix. The crystallographically distinct Yb(III) ion is ligated to six oxygen atoms from the three bis-β-diketones and two oxygen atoms from DMSO. The Yb–O distances are in the range of 2.289(2)–2.352(1) Å, which are longer than values in mononuclear **1**. The Yb···Yb distance in the same helicate is 13.0 Å. The formation of helicate requires the ligands to undergo helication twisting to wrap about the metal ions. The extent of the twisting of ligands is mainly controlled by the principle of stereochemical matching.[27] In the self-assembly processes of **2**, one of the three stranded ligands adopts cis-, while it is trans- for the rest two. The dihedral angles between the two thiophene planes in trans-conformation are 18.6° and 20.9°, whereas it increases to 45.2° in cis-conformation. With respect to the trans-conformation, the small torsion angles make the ligand exist large tension, and looks like an "arch" (Figure S3). In addition, it is interesting to observe the occurrence of C–H···F interactions in **1** and **2**, which have been implicated in the stabilization of the molecules structures and conformational preference (Figure S4).[28] Meanwhile, π···π interaction is found between the thienyl rings of the adjacent helicate in complex **2**. The whole structure of **2** is stabilized through the combination of π–π and C–H···F interactions.

UV–Vis Spectra

UV–Vis absorption spectra of the ligands TTA, BTT and their corresponding Yb(III) complexes in dimethyl sulfoxide (DMSO) solution are shown in Figure 2. TTA and BTT exhibit two broad, intense absorption transitions in the spectral range of 250–500 nm. The formers are attributed to the $^1\pi$–π^* transition in thiophene and bithiophene groups. The others are attributed to the singlet–singlet $^1\pi$–π^* transition of the β-diketone moieties, with maxima bands λ_{max} = 337 nm and 397 nm for TTA and BTT, respectively. In comparison to the ligands, the absorption maxima of **1** and **2** present small blue shifts by 3 nm and 6 nm, respectively. Moreover, the spectral patterns of the complexes are similar to that of the free ligand, indicating that the coordination of the lanthanide ions play a very minor role on the ground states properties of the ligands. The molar absorption coefficient values of **1** and **2** are calculated to be 0.71×10^5 (337 nm) and 1.41×10^5 (397 nm) $L \cdot mol^{-1} \cdot cm^{-1}$, respectively.

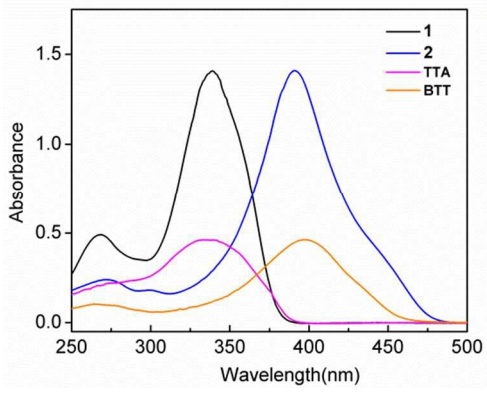

Figure 2 UV–Visible absorption spectra of the ligands TTA, BTT, **1** and **2** in DMSO ($c = 2.0 \times 10^{-5}$ M for TTA, **1**; $c = 1.0 \times 10^{-5}$ M for BTT, **2**).

Photoluminescent properties of the complexes

The photophysical properties of the Yb(III) complexes were investigated in DMSO with the same Yb(III) ions concentration at room temperature. The excitation spectra of complexes were recorded by monitoring the maximum emitting bands at 975 nm (Figure 3). The excitation spectra of mono- and bis-β-diketone complexes show bands in the range of 318–390nm and 330–480 nm, respectively, which match the corresponding absorption spectra confirming the energy transfer takes place from the ligands to Yb(III) ions. Notably, the excitation band of bis-β-diketone complex extends from UV to the visible range (420–480nm), which is especially important for the materials employed in bioanalysis and bioimaging, since living tissue are usually damaged by UV light.[29]

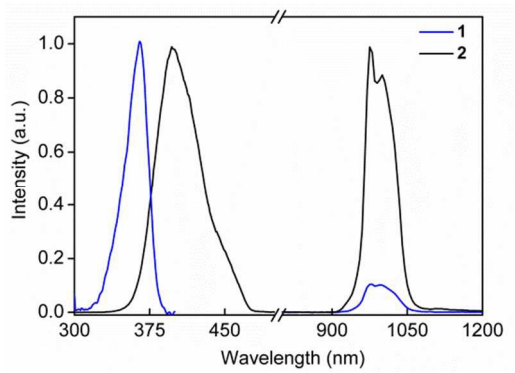

Figure 3 Excitation (left) and emission (right) spectra of **1** and **2** in DMSO.

The emission spectra of $Yb(TTA)_3(DMSO)$ and $Yb_2(BTT)_3(DMSO)_4$ in DMSO are shown in Figure 3. Upon excitation with the isoabsorptive band at 368 nm (Figure 2), the characteristic emission of Yb(III) ion corresponding to the $^2F_{5/2}$–$^2F_{7/2}$ transition at 900–1100 nm is observed for their complexes. In order to conveniently compare their luminescent intensity, the maximum emitting intensity of **2** at 975 nm is normalized. As shown in Figure 3, the bis-β-diketone complex displays about 10 times higher signal intensity than the mono-β-diketone complex. Taking the $Yb(TTA)_3(H_2O)_2$ as reference,[30] the values of emission quantum yields (Φ_{tot}) of two complexes in DMSO were calculated to be 0.24% for **1** and 2.35% for **2**, respectively. The value of **2** is comparable to those highly luminescent Yb(III) complexes with the azulene and 8-hydroxyquinolines ligands.[31] However, the more important issue should be the reason why the helicate gives so large enhancement of luminescence intensity in comparison to the mononuclear complex?

It is well-known that the luminescence quantum yield of the complexes upon excitation of the organic ligand is determined by the efficiency of the energy transfer (η_{ET}) and the intrinsic quantum yield (Φ_{Ln}) of the lanthanide luminescence (eqn. 1)

$$\Phi_{tot} = \eta_{ET}\Phi_{Ln} \quad (1)$$

According to this equation, simultaneously optimizing the two parameters is crucial in the development of systems that result in high quantum yields from lanthanide centered emission. The intrinsic quantum yields of Yb(III) ion luminescence could be estimated using the equation 2, after the calculation of the radiative lifetime (τ_{rad}) from the absorption spectra of Yb(III) ion (Figure 4) with a modified Einstein equation (equ. 3):[32]

$$\Phi_{Ln} = \frac{k_r}{k_r + k_{nr}} = \frac{\tau_{obs}}{\tau_{rad}} \quad (2)$$

$$\frac{1}{\tau_{rad}} = k_r = 2303 \times \frac{8\pi c n^2 \tilde{\nu}_m^2 (2J+1)}{N_A(2J'+1)} \int \varepsilon(\tilde{\nu}) d\tilde{\nu} \quad (3)$$

$$\tilde{\nu}_m = \frac{\int \tilde{\nu} \cdot \varepsilon(\tilde{\nu}) d\tilde{\nu}}{\int \varepsilon(\tilde{\nu}) d\tilde{\nu}}$$

Where, N_A is Avogadro's number, c is the speed of light in centimeters per second, J and J' are the quantum numbers for the ground and excited states, respectively. $\int(\tilde{\nu})d\tilde{\nu}$ is the integrated spectrum of the f–f transition, $\tilde{\nu}_m$ is the barycenter of the transition, and n = 1.4795 for DMSO. The calculated values of the radiative lifetime (τ_{rad}) are 534 μs for mononuclear **1** and 338 μs for binuclear **2.**

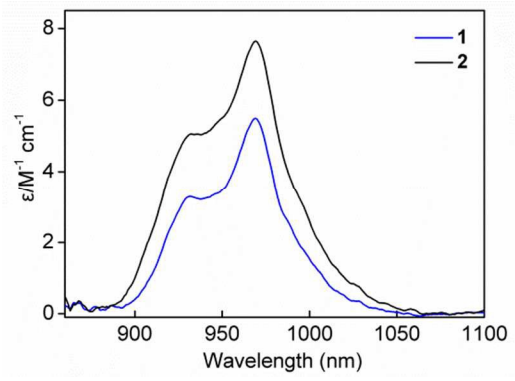

Figure 4 Near-infrared spectra of f–f absorption transition for **1** and **2** in DMSO.

The observed lifetimes (τ_{obs}) were determined by monitoring the emission decay curves within the $^2F_{5/2}$–$^2F_{7/2}$ transition at 975 nm. Typical decay profiles of **1** and **2** are shown in Figure S5. The two decay curves are well-reproduced by single-exponential functions, indicating that only one species exists in the excited state of the complexes. The lifetimes of **1** and **2** were found to be 2.45 μs and 14.19 μs, respectively. With the calculated radiative lifetimes (τ_{rad}) and the observed lifetimes (τ_{obs}), the intrinsic quantum yields (Φ_{Ln}, eqn.1) are found to be 0.46% and 4.20% for **1** and **2**, respectively. Obviously, the bis-β-diketone complex **2** shows about 10 times higher intrinsic quantum yield than the mono-β-diketone complex **1**, and the increasing magnitude is in accord with the observed luminescence quantum yield (Φ_{tot}). With the observed and intrinsic quantum yields, the sensitised efficiencies (η_{ET}, eqn. 2) are found to be 52% and 58% for **1** and **2**, respectively. The similarity in sensitised efficiency makes it not important to further investigate the excited mechanisms for Yb(III) luminescence. Based on above results, it can be confirmed that the remarkable enhancement of luminescence quantum yield for bis-β-diketone complex origins from its higher intrinsic quantum yield than the mono-β-diketone complex.

The intrinsic quantum yield is the result of radiative transition that competes with the nonradiative transition processes (eqn. 2). Thus, it indicates the appearance of the more dominantly radiative transition to nonradiative transition in **2** than that in **1**. By using the radiative lifetimes, the radiative rate constants (k_r) are calculated to be 1870 $s^{-1}$and 2956 s^{-1} for **1** and **2**, respectively (eqn. 3). According to eqn. 2, the nonradiative rate constants are calculated to be 4.05 × 10^5 s^{-1} and 6.74 × 10^4 s^{-1} for **1** and **2**, respectively. Generally, the reduction of the geometrical symmetry of the coordination structure leads to a large radiative rate constants.[33] By utilizing the SHAPE 2.1 software, the coordination configurations were

found to be capped octahedron (COC–7, C_{3v}) for **1** and square antiprism (SAPR–8, D_{4d}) for **2**. Obviously, the Yb(III) ions in mononuclear complexes locate at a lower symmetry environment than that in helicates. Thus, the previous empirical law seems not to be suitable for this system. This deviation probability origins from the variation of metal ions coordination configuration in solution, or different coordination numbers of Yb(III) ions.[34]

In comparison to 1.6 times enhancement of radiative rate constant, the helicate **2** displays 6.0 times decrease of the nonradiative rate constant to mononuclear analogue. It indicates that the nonradiative transition plays more important roles for deactivating the excited state of Yb(III) ions in **1**. It is well-known that the quenching of lanthanide excited state by nonradiative transition is mainly caused by high-energy oscillators, such as C–H and O–H bonds present in ligands or solvents. The energy loss from the excited state of Ln(III) ions to vibrational energy of a solvent molecule or ligand has been proposed to occur according to Förster energy transfer mechanism.[35] The energy transfer rate, k_{12} between the two centers is inversely proportional to the distance between the two centers, r (eqn. 4), while is proportional to the multipole-multipole Coulombic interaction factor, C_{d-d} (eqn. 5). Where $\tilde{v}$ is the energy of the resonant transition, $g_1(\tilde{v})$ and $g_2(\tilde{v})$ are the normalized lineshapes of the emission and absorption transition respectively, and f_1 and f_2 are the oscillator strengths of the emission transition of the Ln(III) ions and the absorption of the vibrational transition of the oscillator.

$$K_{12} = C_{d-d} r^{-6} \qquad (4)$$

$$C_{d-d} = \left[\frac{(3e^4 f_1 f_2)}{8\pi^2 m^2 c^3 n^4 \tilde{v}^2}\right] \int g_1(\tilde{v}) g_2(\tilde{v}) d\tilde{v} \qquad (5)$$

According to eqn. 4, the quenching efficiency of oscillators to the lanthanide luminescence significantly depends on the distance between them. Thus, we firstly compared the distances of metal center to the oscillators. Due to high energy of C–H vibrations, the distance of Yb–C···H are firstly measured from the single crystal structures, and the values are summarized in Table S2. Herein, we classify the C–H bonds into three types by the distance of the metal center to C–H bonds, namely the nearest methine, the modest methyl in DMSO, and the farthest C–H in thiophene rings. As shown in Table S2, the average distances of Yb(III) to the carbon atoms of three types of C–H bonds are very close in two complexes. The distance differences between the same types of Yb–C in two complexes are in range of 0.006–0.099 Å. So small changes of Yb–C distances indicate that the C–H quenching effects on Yb(III) luminescence in two complexes should be similar. In view of the low energy gap between the excited state and the ground state of Yb(III) ion, the quenching effects of harmonics of other lower frequent oscillators, such as C=O, C=C and C–O, etc. are also considered. The distances of metal to these oscillators show similar case as observed in C–H species. Therefore, the effect of the distances of metal centers to oscillators on nonradiative transition should also be similar in two complexes.

On the other hand, the quenching efficiency of oscillators to Ln(III) ion emitting state is proportional to the oscillator strengths (f_2) of absorption of the vibrational transition (eqn. 5), which can be estimated using eqn. (6) after the calculation of the molar extinction coefficient, ε (eqn. 7):

$$f = 4.33 \times 10^{-9} \int \varepsilon_v \, dv \qquad (6)$$

$$\varepsilon = \frac{1}{cl} \lg\left(\frac{T_0}{T}\right) \qquad (7)$$

According to the eqn. (6) and (7), the f_2 is inversely proportional to transmittance T% of the vibrational bands. Therefore, the lower T% of the bands in IR regions reflects the higher quenching effect of oscillators on the excited state of lanthanides. In order to compare the oscillator strengths of the same bands, we assumed that the C–F bonds at 1303 cm^{-1} have the same vibration intensity in two complexes, and the T% is normalized as interior reference. It is rational to consider that the two ligands have similar molecule structure, and the C–F bond locate at the terminal of ligands, where the variations of molecule dipolar moment have least influences to this bond. With this assumption, the intensities of same bands of the complexes are compared, and attributed in details.

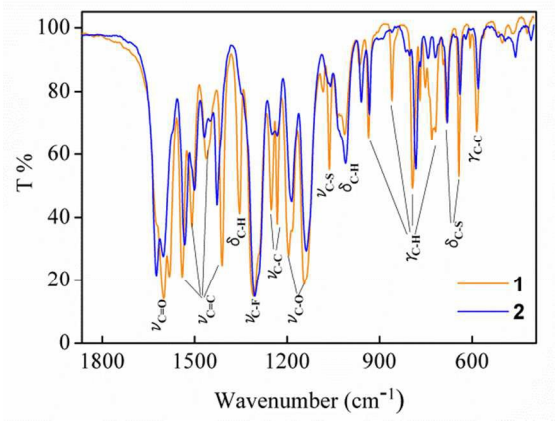

Figure 5 FT–IR spectra of the complexes (**1**, orange line; **2**, blue line).

As shown in Figure 5, the vibration bands at 1626–1583 cm^{-1} are attributed to C=O stretching vibration of the ligands. In **1**, the band red shifts by 10 cm^{-1} compared with that in **2**, which is attributed to the shorter Yb–O bond length. The shorter distance of metal cation to the oxygen atom decrease the electron density of the coordinated atoms, and thus the decreasing C=O vibrational energy. Due to exhibiting keto-enol tautomerism in two β-diketones, C–O stretching vibrations are observed in range of 1195–1187 cm^{-1} and 1145–1141 cm^{-1}, and the keto-enol tautomerism C=C stretching vibrations present at 1540–1532 cm^{-1} and 1470–1462 cm^{-1}. Whereas, the C=C stretching vibrations of thiophene rings present at 1509–1501 cm^{-1} and 1424–1408 cm^{-1}. The C–C stretching vibrations of diketone units and thiophene rings present at 1250–1230 cm^{-1},

while the out-of-plane bending modes of ring present at about 580 cm^{-1}. Apart from the high frequent stretching vibrations of C–H, the in- and out-of-plane bending vibrations of C–H can also be observed at 1354 cm^{-1}, 1009–1013 cm^{-1}, and 862–719 cm^{-1}, 936–932 cm^{-1}, which are attributed to the methines of diketone units and thiophene rings, respectively. In addition, the peaks at 1060 cm^{-1} and 684–642 cm^{-1} are attributed to the C–S stretching and bending vibration due to the involving of DMSO in the coordination sphere. According to above comparisons, it is clearly observed that the two complexes have very similar spectral pattern, and slight variation of absorption position. However, an obvious difference for two complexes is that all the absorption intensities in TTA are almost overwhelmingly stronger than that observed in BBT. The larger oscillator strengths present in **1** undoubtedly lead to the faster nonradiative rate, and thus decrease luminescence quantum yield of Yb(III) ion. The lower oscillator strengths in **2** should benefit from its helical structure. From the crystal structure, we can easily observe that the two of three strands ligands keep a tensive arched pattern. It means that a large tension exists in the helicates, and furthest restrict the stretching or bending vibration of the bonds.

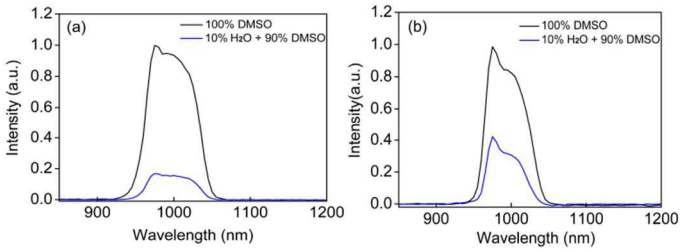

Figure 6 Emission spectra of **1** (a) and **2** (b) before and after the addition of 10% volume water into DMSO.

Apart from intramolecular oscillators, the deactivation of the excited state of Yb(III) ion by high energy oscillators present in solvents were also examined. It is well document that the designing of sterically demanding ligands that encapsulate the metal within a hydrophobic shell is an effective strategy to decrease the nonradiative transition caused by the solvents.[36] In order to examine the encapsulation properties of mononuclear structure and binuclear helical structure to the metal ions, the 10% volume of water is added into the DMSO solutions of the two complexes. As shown in Figure 6, the luminescence intensities of Yb(III) ion at 975 nm decreased by 83% and 58% for **1** and **2**, respectively. The large water quenching effect in **1** indicates that waters molecules are more prone to access the coordination sphere of the lanthanide ions. According to the crystal structure, it can be observed that mononuclear complex has completely open 3D space for solvents entering into the second coordination sphere. In the case of **2**, the formation of helicate effectively decreases the probability of solvents entering into the inner space of helicate. It follows that the helicates display obvious advantage for protecting the metal ion from deleterious solvent molecules.

Conclusion

In summary, we have designed a new bis-β-diketone ligand (BTT) by coupling of two mono-β-diketone (TTA) at the 5,5'-position of thiophene ring, which forms triple-stranded binuclear structure with the Yb(III) ion in a 3:2 ratio of ligand to metal. The luminescence quantum yields experiment reveals that the dinuclear complex has about 10 times luminescent enhancement compared with the mononuclear analogue. This enhancement is attributed to several factors depending on the structure: i) the faster radiative rate constant; ii) part-shielding the ion from the solvent molecules by encapsulation with the helicate to form a protecting shell around the ion; iii) the reducing oscillator strengths of absorption of the vibrational transition due to the tension caused by the helical twisting of ligands in helicate. Based on above analysis, we can conclude that the bright luminescence of the bis-β-diketone complex mainly results from the efficiently restricting the nonradiative transition caused by the oscillators in ligands and solvents. These results show the importance of the designing of the helicate for enhancing the lanthanide ions NIR luminescence.

Experimental

Materials and instruments

The commercially available chemicals were analytical reagent grade and used without further purification. $YbCl_3 \cdot 6H_2O$ was prepared according to the literature by dissolving 99.99% oxide in a slight excess of hydrochloric acid. The solution was evaporated and the precipitate was collected from water.

Elemental analyses were performed on an Elementar Vario EL cube analyzer. FT-IR spectra were obtained on a Perkin-Elmer Spectrum One spectrophotometer by using KBr disks in the range of 4000–450 cm^{-1}. UV spectra were recorded on a Perkin-Elmer Lambda 25 spectrometer. Thermal analyses were conducted on a Perkin-Elmer STA 6000 with a heating rate of 10 ºC·min^{-1} in a temperature range from 30 ºC to 800 ºC. The ^1H NMR spectra was recorded on a Bruker Avance III 400 MHz spectrometer in $CDCl_3$ solution. Electron ionization (EI) and Electrospray time-of-flight (ESI-TOF) mass spectra were recorded on Agilent 5973N and Bruker maXis mass spectrometers, respectively. Crystal data of the complexes were collected on a Xcalibur, Eos, Gemini diffractometer with Mo Kα radiation (λ = 0.71073 Å). All data were collected at a temperature of 23 ± 2 ºC. The structures were solved by the direct methods and refined on F^2 by full-matrix least-squares using the SHELXTL-97 program. The Yb(III) ions were easily located and then non-hydrogen atoms (C, S, O and F) were placed from the subsequent Fourier-difference maps. All non-hydrogen atoms were refined anistropically. The data collection and refinements were given in Table S1. Excitation and emission spectra were measured with an Edinburgh FLS 920 fluorescence spectrophotometer. Luminescence lifetimes were recorded on a single photon counting spectrometer from Edinburgh Instrument (FLS 920) with a microsecond pulse lamp as the excitation sources. The data were analyzed by

software supplied by Edinburgh Instruments. The luminescence quantum yields of the complexes were measured in DMSO at room temperature (λ_{exc} = 368 nm, A = 0.045) and cited relative to a reference solution of $[Yb(TTA)_3(H_2O)_2]$ (Φ = 0.35 %), and were calculated according to the well-known equation:

$$\Phi_{overall} = \frac{n^2 A_{ref} I}{n_{ref}^2 A I_{ref}} \Phi_{ref}$$

Where n, A, and I denote the refractive index of solvent, the absorbance at the excitation wavelength, and the area of the emission spectrum, respectively, and Φ_{ref} represents the quantum yield of the standard $[Yb(TTA)_3(H_2O)_2]$ solution. The subscript *ref* denotes the reference, and the absence of a subscript implies an unknown sample.

Synthesis of 5,5'-diacetyl-2,2'-bithienyl. 5,5'-Diacetyl-2,2'-bithienyl was prepared according to the process described in the literature. Five drops of 85% phosphoric acid were added to a refluxing solution of bithienyl (2.1 g, 12.6 mmol) in 25 mL of acetic anhydride and the boiling continued for one hour. The hot solution was poured on 200.0 g of ice and stirred until the acetic anhydride had hydrolyzed. The green crystals were removed by filtration and recrystallized once from 75 mL of dioxane to give the desired compound as pale yellow flakes (2.4 g, 77%). Anal. Calc. for $C_{12}H_{10}O_2S_2$ (250.34): C, 57.57; H, 4.03; O, 12.78; S, 25.62. Found: C, 57.49; H, 4.11; O, 12.74; S, 25.56. ESI–MS m/z 250.32 M^+.

Synthesis of 5,5′-bis(4,4,4-trifluoro-1,3-dioxobutyl)(2,2'-bithienyl), BTT. A mixture of sodium hydride (0.8 g, 20 mmol) and ethyl trifluoroacetate (2.9 g, 20 mmol) in 40 mL dry DME (ethylene glycol dimethyl ether) was stirred for 10 min, followed by the addition of 5,5'-Diacetyl-2,2'-bithienyl (2.1 g, 8.4 mmol), which was further stirred at room temperature for 24 h (Scheme 1). The resulting mixture was poured into 100 mL ice-water and acidified to pH = 2–3 using hydrochloric acid (2 M), the resulting orange precipitate was filtered and dried in vacuum. Recrystallization from toluene gave orange needle crystals (2.2 g, 59%). Anal. Calc. for $C_{16}H_8F_6O_4S_2$ (441.98): C, 43.44; H, 1.82; O, 14.47; S, 14.50. Found: C, 43.49; H, 1.89; O, 14.54; S, 14.39. IR (KBr, cm^{-1}): 3662 (m), 3097 (w), 1603 (s), 1542 (s), 1446 (w), 1469 (w), 1408 (m), 1339 (m), 1303 (s), 1238 (m), 1219 (m), 1175 (s), 1138 (s), 1045 (w), 941 (w), 921 (w), 855 (w), 782 (m), 705 (w), 672 (w), 635 (w), 575 (w). ^1H NMR ($CDCl_3$, 400 MHz): 12.09 (s, 2H), 8.37 (s, 2H), 7.79 (s, 2H), 6.99 ppm (s, 2H). ESI–MS m/z 441.95 $[M + H]^+$.

Synthesis of $Yb_2(BTT)_3(DMSO)_4$. BTT (100.2 mg, 0.23 mmol) and triethylamine (46.1 mg, 0.46 mmol) were dissolved in 10 mL hot EtOH. To this solution cooled to room temperature, $YbCl_3 \cdot 6H_2O$ (62.0 mg, 0.16 mmol) in 10 mL EtOH was added dropwise to the solution and stirred 24 h (Scheme 1). The precipitate formed after the addition of water was filtered and dried in vacuum (75%). Single crystals suitable for X-ray analyses were obtained by slow diffusion of n-hexane into chloroform/DMSO solution of the complex. Anal. Calc. for $C_{56}H_{42}F_{18}O_{16}S_{10}Yb_2$ (1983.86): C, 41.02; H, 2.95; O, 15.61; S, 19.56; F, 20.86. Found: C, 41.05; H, 2.98; O, 15.69; S, 19.60; F, 20.89. IR (KBr, cm^{-1}): 2813 (w), 1626 (s), 1604 (s), 1534 (s), 1500 (w), 1462 (w), 1428 (w), 1302 (s), 1248 (w), 1235 (w), 1189 (m), 1138 (m), 1058 (w), 1012 (w), 932 (w), 781 (m), 680 (w), 638 (w). ESI–MS m/z 1694.80 $[Yb_2(BTT)_3 + Na]^+$.

Synthesis of Yb(TTA)$_3$(DMSO). TTA (100.2 mg, 0.45 mmol) and triethylamine (91.2 mg, 0.90 mmol) were dissolved in 10 mL EtOH. To this solution, $YbCl_3 \cdot 6H_2O$ (58.1 mg, 0.15 mmol) in 10 mL EtOH was added dropwise to the solution and stirred 24 h. The precipitate formed after the addition of water was filtered and dried in vacuum (71%). Single crystals suitable for X-ray analyses were obtained by slow diffusion of n-hexane into chloroform/DMSO solution of the complex. Anal. Calc. for $C_{26}H_{18}F_9O_7S_4Yb$ (917.94): C, 41.93; H, 2.84; O, 15.04; S, 17.22; F, 22.96. Found: C, 41.94; H, 2.87; O, 15.05; S, 17.28; F, 23.01. IR (KBr, cm^{-1}): 2920 (w), 2849 (w), 1605 (s), 1580 (s), 1538 (s), 1508 (m), 1462 (w), 1412 (s), 1357 (m), 1302 (s), 1248 (m), 1231 (m), 1197 (s), 1142 (s), 1059 (m)，1004 (w), 932 (w), 861 (w) 794 (m), 726 (w), 680 (w), 642 (m), 583 (w). ESI–MS m/z 862.92 $[Yb(TTA)_3 + Na]^+$.

Acknowledgements

This work is financially supported by the National Natural Science Foundation of China (Nos. 51302068 & 51472076).

Notes and references

Key Laboratory of Functional Inorganic Material Chemistry (Heilongjiang University), Ministry of Education, School of Chemistry and Materials Science, Heilongjiang University, Harbin 150080, PR China. Fax: 86-451-86608715 E-mail: lhf4612@163.com; yanpf@vip.sina.com

Electronic Supplementary Information (ESI) available: ^1H NMR spectra of ligands, TG patterns, CCDC reference numbers 1428241 and 948140 for **1** and **2**. See DOI:10.1039/b000000x/

1 (a) X. H. Wang, H. J. Chang, J. Xie, B. Z. Zhao, B. Liu, S. L. Xua, W. B. Pei, N. Ren, L. Huang and W. Huang, *Coord. Chem. Rev.*, 2014, **273**, 201–212; (b) J.-C. G. Bünzli and S. V. Eliseeva, *Chem. Sci.*, 2013, **4**, 1939–1949; (c) H. Xiang, J. Cheng, X. Ma, X. Zhou and J. J. Chruma, *Chem. Soc. Rev.*, 2013, **42**, 6128–6185; (d) S. V. Eliseeva and J.-C. G. Bünzli, *Chem. Soc. Rev.*, 2010, **39**, 189–227.

2 (a) A. J. Amoroso and S. J. A. Pope, *Chem. Soc. Rev.*, 2015, **44**, 4723–4742; (b) M. C. Heffern, L. M. Matosziuk and T. J. Meade, *Chem. Rev.*, 2014, **114**, 4496–4539; (c) J.-C. G. Bünzli, S. Comby, A.-S. Chauvin, C. D. B. Vandevyver, *J. Rare Earth*, 2007, **25**, 257–274; (c) J.-C. G. Bünzli, *Chem. Rev.*, 2010, **110**, 2729–2755.

3 (a) E. Hemmer, N. Venkatachalam, H. H. A. A. Hattori, Y. Ebina, H. Kishimotoa and K. Sogaa, *Nanoscale*, 2013, **5**, 11339–11361; (b) J.-C. G. Bünzli, *Coord. Chem. Rev.*, 2015, **293**, 19–47.

4 C. Piguet and J.-C. G. Bünzli, *Chem. Soc. Rev.*, 2005, **34**, 1048–1077.

5 (a) S. Comby and J.-C. G. Bünzli, *Handbook on the Physics and Chemistry of Rare Earths*, Elsevier: Amsterdam, 2007, **37**, 217–470; (b) A. Beeby, I. M. Clarkson, R. S. Dickins, S. Faulkner, D. Parker, L. Royle, A. S. de Sousa, J. A. G. Williams and M. Woods, *J. Chem. Soc., Perkin Trans. 2.*, 1999, 493–504.

6 (a) S. W. Magennis, S. Parsons and Z. Pikramenou, *Chem. Eur. J.*, 2002, **8**, 5761–5771; (b) P. E. Ryan, L. Guénée, G. Canard, F. Gumy, J.-C. G. Bünzli and C. Piguet, *Inorg. Chem.*, 2009, **48**, 2549–2560; (c)

E. R. Trivedi, S. V. Eliseeva, J. Jankolovits, M. M. Olmstead, S. Petoud and V. L. Pecoraro, *J. Am. Chem. Soc.*, 2014, **136**, 1526–1534; (d) B. L. Reid, S. Stagni, J. M. Malicka, M. Cocchi, G. S. Hanan, M. I. Ogden and M. Massi, *Chem. Commun*., 2014, **50**, 11580–11582.

7 (a) G. Mancino, A. J. Ferguson, A. Beeby, N. J. Long and T. S. Jones, *J. Am. Chem. Soc.*, 2005, **127**, 524–525; (b) Y. Peng, H. Q. Ye, Z. Li, I. Hernández, W. P. Gillin and P. B. Wyatt, *J. Phys. Chem. Lett*., 2014, **5**, 1560–1563; (c) H. Q. Ye, Z. Li, C. C. Wang, Y. X. Zheng, M. Motevalli, P. B. Wyatt, W. P. Gillin and I. Hernández, *J. Phys. Chem. C*, 2013, **117**, 23970–23975.

8 W. T. Carnall, *Handbook on the Physics and Chemistry of Rare Earths*, Elsevier: Amsterdam, 1979, **3**, 172–205.

9 (a) X. S. Ke, B. Y. Yang, X. Cheng, S. L.-F. Chan and J. L. Zhang, *Chem. Eur. J.*, 2014, **20**, 4324–4333; (b) T. Zhang, C.-F. Chan, R. F. Lan, H. G. Li, N.-K. Mak, W.-K. Wong and K.-L. Wong, *Chem. Commun.*, 2013, **49**, 7252–7254.

10 (a) M. V. López, S. V. Eliseeva, J. M. Blanco, G. Rama, M. R. Bermejo, M. E. Vázquez and J.-C. G. Bünzli, *Eur. J. Inorg. Chem.*, 2010, **28**, 4532–4545; (b) M. Andrews, J. E. Jones, L. P. Harding and S. J. A. Pope, *Chem. Commun*., 2011, **47**, 206–208.

11 (a) C. Doffek and M. Seitz, *Angew. Chem. Int. Ed*., 2015, **54**, 9719–9721; (b) J. E. Jones and S. J. A. Pope, *Dalton Trans*., 2009, **39**, 8421–8425.

12 P. Marta, L. Jerzy and L. Tadeusz, *Dalton Trans*., 2006, 381–388.

13 L. R. MacGillivray, J. L. Reidb and J. A. Ripmeesterb, *Chem. Commun*., 2001, 1034–1035.

14 X. M. Guo, H. D. Guo, L. S. Fu, L. D. Carlos, R. A. S. Ferreira, L. N. Sun, R. P. Deng and H. J. Zhang, *J. Phys. Chem. C*, 2009, **113**, 12538–12545.

15 M. Albrecht, O. Osetska, R. Fröhlich, J.-C. G. Bünzli, A. Aebischer, F. Gumy and J. Hamacek, *J. Am. Chem. Soc*., 2007, **129**, 14178–14179.

16 S. I. Klink, L. Grave, D. N. Reinhoudt and F. C. J. M. van Veggel, *J. Phys. Chem. A*, 2000, **104**, 5457–5468.

17 S. Quici, M. Cavazzini, G. Marzanni, G. Accorsi, N. Armaroli, B. Ventura and F. Barigelletti, *Inorg. Chem*., 2005, **44**, 529–537.

18 G. A. Hebbink, S. I. Klink, L. Grave, P. G. B. O. Alink and F. C. J. M. van Veggel, C*hemPhysChem*., 2002, **3**, 1014–1018.

19 J. Zhang, P. D. Badger, S. J. Geib and S. Petoud, *Angew. Chem. Int. Ed*., 2005, **44**, 2508–2512.

20 P. B. Glover, A. P. Bassett, P. Nockemann, B. M. Kariuki, R. V. Deun and Z. Pikramenou, *Chem. Eur. J*., 2007, **13**, 6308–6320.

21 (a)J. H. Ryu, Y. K. Eom, J.-C. G. Bünzli and H. K. Kim, *New J. Chem*., 2012, **36**, 723–731; (b) R. F. Ziessel, G. Ulrich, L. Charbonniére, D. Imbert, R. Scopelliti and J.-C. G. Bünzli, *Chem. Eur. J.*, 2006, **12**, 5060–5067.

22 (a) K. Binnemans, *Handbook on the Physics and Chemistry of Rare Earths*, Elsevier: Amsterdam, 2005, **35**, 107–272; (b) S. Biju, Y. K. Eom, J.-C. G. Bünzli and H. K. Kim, *J. Mater. Chem. C*, 2013, **1**, 3454–3466; (c) J. Feng and H. J. Zhang, *Chem. Soc. Rev*., 2013, **42**, 387−410; (d) Z. Ahmed and K. Iftikhar, *J. Phys. Chem. A*, 2013, **117**, 11183−11201.

23 (a) P. Martín-Ramos, P. S. P. da Silva, V. Lavín, I. R. Martín, F. Lahoz, P. Chamorro-Posada, M. R. Silva and J. Martín-Gil, *Dalton Trans.*, 2013, **42**, 13516–13526; (b) Z. Ahmed and K. Iftikhar, *Polyhedron*, 2015, **85**, 570−592; (c) J. Feng, J. B. Yu, S. Y. Song, L. N. Sun, W. Q. Fan, X. M. Guo, S. Dang and H. J. Zhang, *Dalton Trans.*, 2009, 2406–2414.

24 J. Y. Li, H. F. Li, P. F. Yan, P. Chen, G. F. Hou and G. M. Li, *Inorg. Chem*., 2012, **51**, 5050–5057.

25 (a) T. Y. Zhu, P. Chen, H. F. Li, W. B. Sun, T. Gao and P. F. Yan, *Phys. Chem. Chem. Phys*., 2015, **17**, 16136–16144; (b) J. Q. Leng, H. F. Li, P. Chen, W. B. Sun, T. Gao and P. F. Yan, *Dalton Trans.*, 2014, **43**, 12228–12235; (c) P. Chen, H. F. Li, W. B. Sun, J. K. Tang, L. Zhang and P. F. Yan, *CrystEngComm*., 2015,**17**, 7227–7232; (d) H. F. Li, P. F. Yan, P. Chen, Y. Wang, H. Xu and G. M. Li, *Dalton Trans.*, 2012, **41**, 900–907; (e) H. F. Li, G. M. Li, P. Chen, W. B. Sun and P. F. Yan, *Spectrochim. Acta Part A.*, 2012, **97**, 197–201; (f) A. P. Bassett, S. W. Magennis, P. B. Glover, D. J. Lewis, N. Spencer, S. Parsons, R. M. Williams, L. D. Cola and Z. Pikramenou, *J. Am. Chem. Soc*., 2004, **126**, 9413–9424.

26 C. Piguet and J.-C. G. Bünzli, *Handbook on the Physics and Chemistry of Rare Earths*, Elsevier: Amsterdam, 2010, **40**, 303–553.

27 C. Piguet, G. Bernardinelli, B. Bocquet, A. Quattropanni and A. F. Williams, *J. Am. Chem. Soc*., 1992, **114**, 7440–7451.

28 (a) G. R. Desiraju, *Chem. Commun*., 2005, 2995–3001; (b) C. R. Jones, P. K. Baruah, A. L. Thompson, S. Scheiner and M. D. Smith, *J. Am. Chem. Soc.*, 2012, **134**, 12064−12071.

29 S. Miwa, S. Yano, Y. Hiroshima, Y. Tome, F. Uehara, S. Mii and E. V. Efimova, *J. Cell. Biochem*., 2013, **114**, 2493–2499.

30 S. B. Meshkova, Z. M. Topilova, D. V. Bolshoy, S. V. Beltyukova, M. P. Tsvirko and V. Y. Venchikov, *Acta Phys. Pol. A*, 1999, **95**, 983–990.

31 (a) N. M. Shavaleev, R. Scopelliti, F. Gumy and J.-C. G. Bünzli, *Inorg. Chem.,*2009, **48**, 7937–7946; (b) J. Zhang and S. Petoud, *Chem. Eur. J*., 2008, **14**, 1264–1272.

32 M. H. V. Werts, R. T. F. Jukes and J. W. Verhoeven, *Phys. Chem. Chem. Phys*., 2002, **4**, 1542–1548.

33 (a) Y. Hasegawa, T. Ohkubo, T. Nakanishi, A. Kobayashi, M. Kato, T. Seki, H. Ito and K. Fushimi, *Eur. J. Inorg. Chem*., 2013, **34**, 5911–5918; (b) K. Miyata, T. Nakagawa, R. Kawakami, Y. Kita, K. Sugimoto, T. Nakashima, T. Harada, T. Kawai and Y. Hasegawa, *Chem. Eur. J.*, 2011, **17**, 521–528; (c) K. Nakamura, Y. Hasegawa, H. Kawai, N. Yasuda, N. Kanehisa, Y. Kai, T. Nagamura, S. Yanagida and Y. Wada, *J. Phys. Chem. A*., 2007, **111**, 3029–3037; (d) Y. Hasegawa, S. Tsuruoka, T. Yoshida, H. Kawai and T. Kawai, *J. Phys. Chem. A.*, 2008, **112**, 803–807; (e) K. Miyata, Y. Hasegawa, Y. Kuramochi, T. Nakagawa, T. Yokoo and T. Kawai, *Eur. J. Inorg. Chem*., 2009, **32**, 4777–4785; (f) K. Binnemans, R. V. Deun, C. Görller-Walrand, S. R. Collinson, F. Martin, D. W. Bruce and C. Wickleder, *Phys. Chem. Chem. Phys.*, 2000, **2**, 3753–3757.

34 N. M. Shavaleev, S. V. Eliseeva, R. Scopelliti and J.-C. G. Bünzli, *Inorg. Chem*., 2015, **54**, 9166–9173.

35 V. S. Ermolaev and E. B. Sveshnikova, *Chem. Phys. Lett*., 1973, **23**, 349–354.

36 Y. T. Yang, J. J. Li, X. J. Liu, S. Y. Zhang, K. Driesen, P. Nockemann and K. Binnemans, C*hemPhysChem*., 2008, **9**, 600–606.

